Proceedings of the Second Workshop Organized by the IAFSS Working Group on Measurement and Computation of Fire Phenomena (MaCFP-2) Gas Phase Subgroup

M. Ahmed[a], F. Brännström[b], A. Brown[c], J.-L. Consalvi[d], J. Floyd[e], G. Forney[f], E. Gissi[g], A. Hamins[f], M. Hansen[c], E. Hawkes[h], J. Hewson[c], J. Hubbard[c], J. Kirsch[c], K. Krishnamurthy[b], I. Leventon[f], J. Lin[h], L. Ma[i,d], G. Maragkos[j], R. McDermott[f], K. McGrattan[f], B. Merci[j], F. Nmira[i], O. Oluwole[k], N. Ren[k], J. Sailer[b], J. Squeo[l], A. Trouvé[a,*], M. Vanella[f], Y. Wang[k], E. Weckman[m], J. Wen[n], B. Wu[k], B. Xu[n], D. Zeng[k], X. Zhao[l], H. Zhou[h]

[a]*Department of Fire Protection Engineering, University of Maryland, College Park, MD 20742, USA*
[b]*Bergische Universität Wuppertal, 42119 Wuppertal, Germany*
[c]*Fire Science and Technology Department, Sandia National Laboratories, Albuquerque, NM 87185, USA*
[d]*Aix-Marseille Université, IUSTI/IMR CNRS 7343, 5 rue E. Fermi, 13453 Marseille Cedex 13, France*
[e]*Jensen-Hughes, Rockville, MD, USA*
[f]*Fire Research Division, National Institute of Standards and Technology, Gaithersburg, MD 20899, USA*
[g]*Corpo Nazionale dei Vigili del Fuoco, Savona, Italy*
[h]*University of New South Wales, Sydney, Australia*
[i]*Direction EDF R&D, 6 quai Watier, 78400 Chatou, France*
[j]*Department of Flow, Heat and Combustion Mechanics, Ghent University-UGent, B-9000 Ghent, Belgium*
[k]*FM Global, Research Division, Norwood, MA 02062, USA*
[l]*Department of Mechanical Engineering, University of Connecticut, Storrs, CT 06269, USA*
[m]*Department of Mechanical and Mechatronics Engineering, University of Waterloo, Waterloo, Ontario, N2L 3G1, Canada*
[n]*Warwick FIRE, School of Engineering, University of Warwick, UK*

Abstract

On April 22, 2021, the "Working Group on Measurement and Computation of Fire Phenomena" (the "MaCFP Working Group") organized its second workshop (MaCFP-2) as a virtual pre-event to the 13th Symposium of the International Association for Fire Safety Science (IAFSS). This report summarizes the main findings of the Gas Phase Phenomena Subgroup's contribution to MaCFP-2; experimental and modeling results prepared by the Condensed Phase Phenomena Subgroup are presented elsewhere. At MaCFP-2, the Gas Phase Phenomena subgroup focused on three target configurations for validation of computational fire models: a Helium plume experiment (Case 1); a methanol pool fire experiment (Case 3); and an ethylene-oxygen-nitrogen experiment (Case 5). Results include discussions of the effects of spatial resolution and of modeling choices (in particular radiation models and soot models).

Keywords: Buoyant plumes, Pool fires, Flame extinction, Fire modeling, Radiation, Soot, Large Eddy Simulation

*Corresponding author
Email address: atrouve@umd.edu (A. Trouvé)

1. Introduction

This report documents the experiments, numerical simulation results, and discussion that took place at the Gas Phase Phenomena Subgroup of the second MaCFP Workshop (MaCFP-2) held on April 22, 2021, as a virtual pre-event to the 13th IAFSS Symposium. Presentations at the workshop provided detailed comparisons between experimental data and computational results obtained by participating modeling groups with the intent to review progress, summarize accomplishments, identify knowledge gaps, and provide guidance with clear objectives for future study. PDF copies of case-specific results and workshop summary presentations are available online (see: https://github.com/MaCFP/macfp-db/releases/tag/macfp-2.0).

The general objective of the MaCFP Working Group is to establish a structured effort in the fire research community in order to make significant and systematic progress in fire modeling through a fundamental understanding of fire phenomena. The technical objectives are to develop the scientific foundations for the detailed understanding and modeling of important fie phenomena (see https://iafss.org/macfp/).

The MaCFP Working Group is a joint effort between experimentalists and modelers on the general topic of the experimental validation of fire models that are based on a Computational Fluid Dynamics (CFD) approach. The MaCFP Working Group is endorsed and supported by the International Association for Fire Safety Science (IAFSS) and is intended as an open, community-wide, international collaboration between fire scientists. The spirit in which MaCFP discussions are conducted is exemplified by the Proceedings of the MaCFP-1 Workshop which was held June 10-11, 2017 in conjunction with the 12th IAFSS Symposium. The proceedings of MaCFP-1 are reported in Ref. [1]. The MaCFP-1 workshop was both a technical meeting for the gas phase subgroup and a planning meeting for the condensed phase subgroup. The gas phase subgroup reported on a suite of experimental-computational comparisons corresponding to a list of five target experimental configurations.

Table 1 provides an overview of current thinking on the key fire dynamics phenomena of interest, which involves the condensed phase, gas phase, and coupled gas and condensed phases. Based on engineering judgement, the phenomena are categorized in terms of their importance in simulating fundamental fire physics. The areas of primary focus include coupled gas phase-condensed phase phenomena such as burning rate (*i.e.,* the fuel mass loss rate), fire growth (*i.e.,* the combustion heat release rate), and flame spread (*i.e.,* the displacement velocity of the flame and pyrolysis regions). The understanding needed to model the primary phenomena are necessary but not sufficient to model the secondary phenomena.

Table 1 also lists the MaCFP benchmark cases that address each relevant phenomenon. The full suite of benchmark cases are given below:

- Gas phase cases:
  Case 1: Turbulent buoyant plumes (Sandia Helium Plume) [2].
  Case 2: Turbulent gaseous pool fires, including:
    Case 2a: NIST McCaffrey natural gas flames [3]
    Case 2b: Sandia 100-cm-diameter methane and hydrogen flames [4, 5].
  Case 3: Turbulent pool fires burning liquid fuel, including:
    Case 3a: Waterloo 30-cm-diameter methanol pool fire [6, 7]
    Case 3b: NIST 30-cm- and 100-cm-diameter methanol pool fires [8–11].
  Case 4: Turbulent gaseous wall fire along a vertical surface (FM Global; methane, ethane, ethylene and propylene) [12, 13]
  Case 5: Turbulent fires burning gaseous fuel under vitiated conditions including:
    Case 5a: FM Global round burner fueled by ethylene [14, 15]
    Case 5b: UMD line burner fueled by methane and propane [16–18]

Table 1: Overview of key fire dynamic phenomena and associated list of benchmark experimental target cases that address the phenomena.

Priority	Phenomena	Benchmark Case
	Coupled Condensed and Gas Phases	
Primary	Burning rate	3
	Fire growth	
	Fire spread	6
Secondary	Suppression	
	Wall-flame interaction	4
	Condensed Phase	
Primary	Ignition	6
	Gasification of condensed fuels	7
	Oxidation	
	Thermal decomposition of solid fuels	6,7
	Gas Phase	
Primary	Buoyant Plumes	1
	Convective heat transfer	3b,6
	Radiative heat transfer	3b,6
	Species composition and transport	3b
	Turbulent flow	3a
	Turbulent mixing	3a
Secondary	Compartment fire effects including ventilation	
	Extinction	5
	Fire temperatures	3
	Instabilities (large and small-scale phenomena)	3a,b
	Re-ignition	5
	Soot formation, growth and oxidation	1
	Toxicity (toxic gas and particle yields)	3b
	Visibility	

- Condensed phase cases:
  Case 6: Fire growth over combustible solids including:

    Case 6a: NIST parallel panel test (PMMA) [19, 20]

    Case 6b: UMD corner wall (SBI) test (PMMA) [21]

  Case 7: NIST Gasification Apparatus (PMMA) [22]

The initial list of target experiments included a number of benchmark configurations that are significant in terms of understanding the dynamics of chemically reacting flows. The target cases were selected to support the strategic interests of the MaCFP exercises (see Table 1). The discussion at MaCFP-1 featured simulations that enable an evaluation of the performance of fire models under high-resolution conditions in which the impact of numerical errors is reduced and many of the discrepancies between experimental data and computational results may be attributed to modeling errors [1]. The experimental databases and the experimental-computational comparisons corresponding to all cases are archived on the MaCFP repository [23] with open access so that the data are available to the fire research community as reference data for future experimental and/or computational studies.

The MaCFP-2 gas-phase target experiments focused on three select configurations in order to be able to dig deeper into analysis. The cases were related to the list above and included Cases 1, 3 and 5. Case 3 was expanded for MaCFP-2 to include both the Waterloo 30 cm methanol pool fire [6] and the NIST 30 cm and 100 cm methanol pool fires [7, 18].

To improve the quality and depth of the comparisons between the different modeling results during MaCFP-2, modeling groups were asked to include the following:

- A grid convergence study for every case, in which the effect of changing spatial resolution in the flow and combustion solver (as opposed to the radiation solver) is quantified.
- For Case 3, the submission includes an angular convergence study in which the effect of changing angular resolution in the radiation solver is quantified.
- Explain their modeling choices for the treatment of the turbulent flow, combustion and radiation transport; modeling groups were encouraged to define a baseline model and apply that model to all simulated cases, and were asked that variations in modeling choices be justified.
- Submit an image of their configuration together with volume rendering of heat release rate and/or temperature/species contours so that those browsing the repository will have a visual reference of the computational results.
- Consider performing (a) fine-grained simulations under high-resolution conditions often preferred by CFD researchers and (b) coarse-grained simulations under moderate-to- marginal resolution conditions (sometimes called VLES) that may be more representative of CFD practitioners.

The following groups submitted computational results for comparisons with experimental data and for discussions at the MaCFP-2:

- Electricité de France (EDF) and Aix-Marseille University (France)
- FM Global (USA)
- Ghent University (UGent, Belgium)
- The Institut de Radioprotection et de Sûreté Nucléaire (IRSN, France)
- The National Institute of Standards and Technology (NIST, USA)
- Sandia National Laboratories (SNL, USA)
- University of Maryland (UMD, USA)
- University of New South Wales (UNSW, Australia)
- University of Warwick (UoW, UK)

These groups used one of the following CFD solvers:

- Code_Saturne developed by EDF [24];
- FDS (Fire Dynamics Simulator) developed by NIST [25];
- FireFOAM based on OpenFOAM [26], developed by FM Global [27];
- fireFPVFoam based on OpenFOAM [26], developed by UNSW [28];
- SIERRA/Fuego developed by SNL [29].

These solvers are representative of current fire modeling capabilities available for research-level and/or engineering-level projects. In the following sections, results for each of the MaCFP-2 cases are discussed.

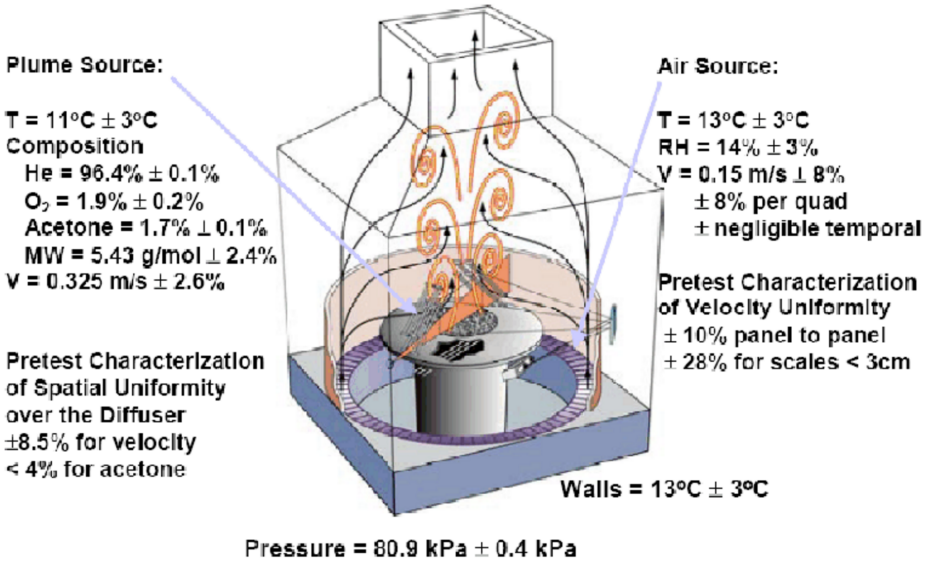

Figure 1: SANDIA helium plume FLAME facility.

1.1. Case 1: Sandia Helium Plume

1.1.1. Experiment

The buoyant plume experiment selected for the first MaCFP workshop is a turbulent non-reacting helium plume studied at a test facility called the Fire Laboratory for the Accreditation of Models by Experimentation (FLAME) facility at Sandia National Laboratories (Sandia) [2, 30]. The original goal of the Sandia buoyant plume experiment was to provide comprehensive turbulent flow velocity and species concentration statistics in a configuration that is representative of large-scale pool fires without the complexities of chemical reactions and temperature variations [2]. The 1 m diameter source provides a plume in the fully-developed turbulent flow regime.

Figure 1 shows the helium plume test setup. The 1 m diameter helium source was surrounded by a 0.51 m wide steel lip, representing the injection plane; this assembly was elevated 2.45 m above an annular ring which introduced a low-velocity co-flow of ambient air [30]. The FLAME facility can be approximated as a 6.1 m cubic chamber covered by a 2.4 m diameter extraction hood. Planar imaging measurements of velocity and species were conducted using Particle Image Velocimetry (PIV) and Planar Laser Induced Fluorescence (PLIF), respectively. Laser measurements were recorded at 200 Hz in a window approximately 0.86 m high and 1.2 m wide, and providing an image of the near-field region (starting from the helium injection plane and centered on the plume centerline). The measurement window includes near-field entertainment zones on both sides of the plume; however, it does not include the lateral and vertical far-field. The experimental uncertainty of the measured velocities and turbulent statistics are reported as 20 % and 30 %, respectively. The uncertainty of the measured helium concentration is reported as 18 %. Inlet conditions are uniform to within 5 % or less for the helium flow and within 10 % for the air coflow. The above uncertainties include run-to-run variability.

For the purpose of MaCFP, tests 25, 29, 32 and 36 were selected corresponding to repeat runs with a helium inlet velocity of 0.339 m/s ± 1.3 %, a flow Reynolds number Re = 3194 ± 0.6 %, a flow Richardson number Ri = 69.53 ± 6.5 % and a measured puffing frequency of 1.45 Hz [2].

1.1.2. Simulations

For MaCFP-2, simulations of the Sandia helium plume were submitted by three groups:

Table 2: Model parameters for Sandia Helium Plume simulations

Institute	Domain	Grid Resolution	Turbulence Model
SNL	5.82 m dia × 9 m ht cylindrical	[R8, R7[A], R6, R5[A], R4] [0.47, 0.58, 0.78, 1.17, 2.33] cm (based on cube root of unstructured fine cell volume)	One-equation k_{sgs}; highly-resolved near-wall LES ($y^+ < 10$); unity Le; $Sc_t = 0.9$
UGent	4 m dia × 4 m ht cylindrical	[1.5, 3, 6, 10, 20] cm non-uniform, based on finest cells concentrated near center	Dynamic Smagorinsky model; dynamic turbulent diffusivity; no wall model (no slip)
NIST	6 m × 6 m × 4 m ht rectangular	[1.5, 3, 6, 10, 20] cm cubic cells	Deardorff (algebraic k_{sgs}); WALE[B] near-wall eddy-viscosity; log law wall stress; constant $Sc_t = 0.5$
NIST2	Full Sandia FLAME facility	[1.25, 2.5, 5, 10] cm cubic cells + unstructured cutcells around non-Cartesian edges	Deardorff (algebraic k_{sgs}); WALE near-wall eddy-viscosity; log law wall stress; constant $Sc_t = 0.5$

[A] Missing root mean squared (rms) data
[B] Wall-adapting local eddy-viscosity (WALE)

Table 3: Reported puffing frequencies (Hz) for Sandia Helium Plume simulations. The mesaured puffing frequency was 1.37 ± 0.18 Hz [2].

Institute	Nominal resolution			
	1.5 cm	3 cm	6 cm	10 cm
SNL	1.38			
UGent	1.46	1.43	1.53[1]	1.20[1]
NIST	1.51	1.35		
NIST2	1.19	1.10		

[1] Dominant modes less prominent.

- National Institute of Standards and Technology (two sets of results: NIST and NIST2);
- Sandia National Laboratories (SNL);
- Ghent University (UGent).

To address questions related to the FLAME facility boundary conditions, the NIST group submitted two sets of results: one with open boundaries; and one with a full model of the FLAME test facility. These results are designated as "NIST" and "NIST2" results, respectively. Key model setup parameters are provided in Table 2; detailed model descriptions (i.e., boundary & initial conditions, submodels, discretization, resolution and computational cost) are available on the MaCFP repository [23]. Selected comparisons of experimental measurements and simulation results are provided in Table 3 and Figs. 2 and 3. Commentary on the results is provided in the next section.

1.1.3. Summary

The Sandia Helium Plume case has been discussed extensively in the first MaCFP workshop [1]. Some major outstanding issues were:

- The grid resolution required to accurately capture the plume dynamics was very fine, compared to engineering practice ($D^*/\Delta x$ on the order of 70, rather than 10 to 20)[1]. This raised the question as to

[1]The characteristic fire diameter is $D^* = (\dot{Q}/[\rho_\infty c_p T_\infty \sqrt{g}])^{2/5}$, where $\dot{Q}$ is the fire's power or heat release rate, ρ_∞ and T_∞ are

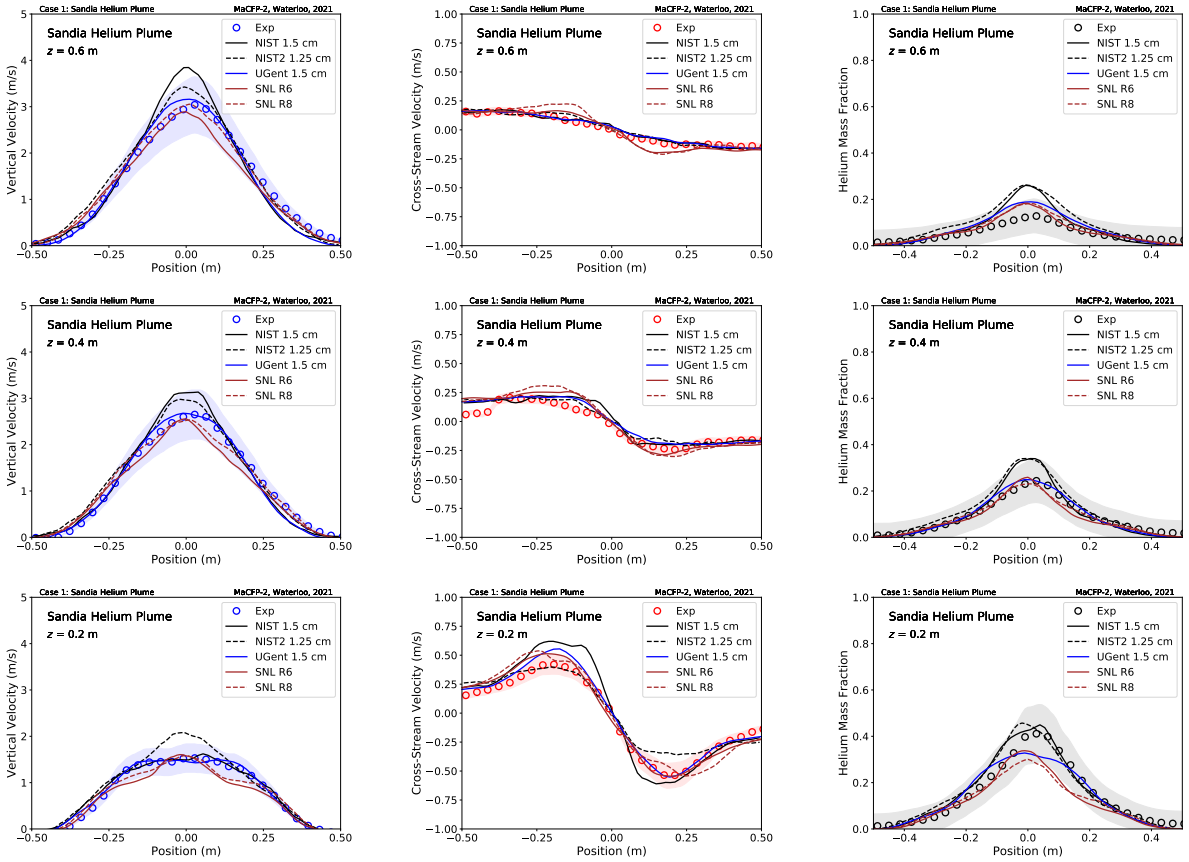

Figure 2: Sandia Helium Plume mean simulation results (nominally 1 cm to 1.5 cm resolution) at heights of 0.2, 0.4, and 0.6 m above the ground plane. Note that "Helium Mass Fraction" data are for Favre-averaged plume fluid. SNL results are for Favre averaged plume fluid, while NIST and UGent results are for ensemble averaged pure helium mass fraction. Lightly colored region corresponds to experimental uncertainty obtained from [31].

whether improvements are possible on coarser grids.

- The agreement between simulation results and experimental data for the helium mass fraction was worse than what could be expected on the basis of flow and mixing fields. That is, with the reasonably accurate prediction of velocity fields (including puffing frequencies), albeit requiring high resolution, we expected better agreement with the scalar fields. This raised the question of whether important details of the plume source were missing, or improvements were necessary for the modelling of subgrid mass transport.

- The exterior was treated with simplified geometrical boundary conditions in the MaCFP 1 submissions. This raised the question whether there would be any benefit to a more detailed representation of the test facility in the exterior boundary conditions.

The first question motivated the use of very coarse meshes in the "UGent" and "NIST" simulations in Table 2. The second question has been resolved in that the experimental data was for pure He mass fraction,

the ambient density and temperature, c_p is the specific heat, and g is the acceleration due to gravity.

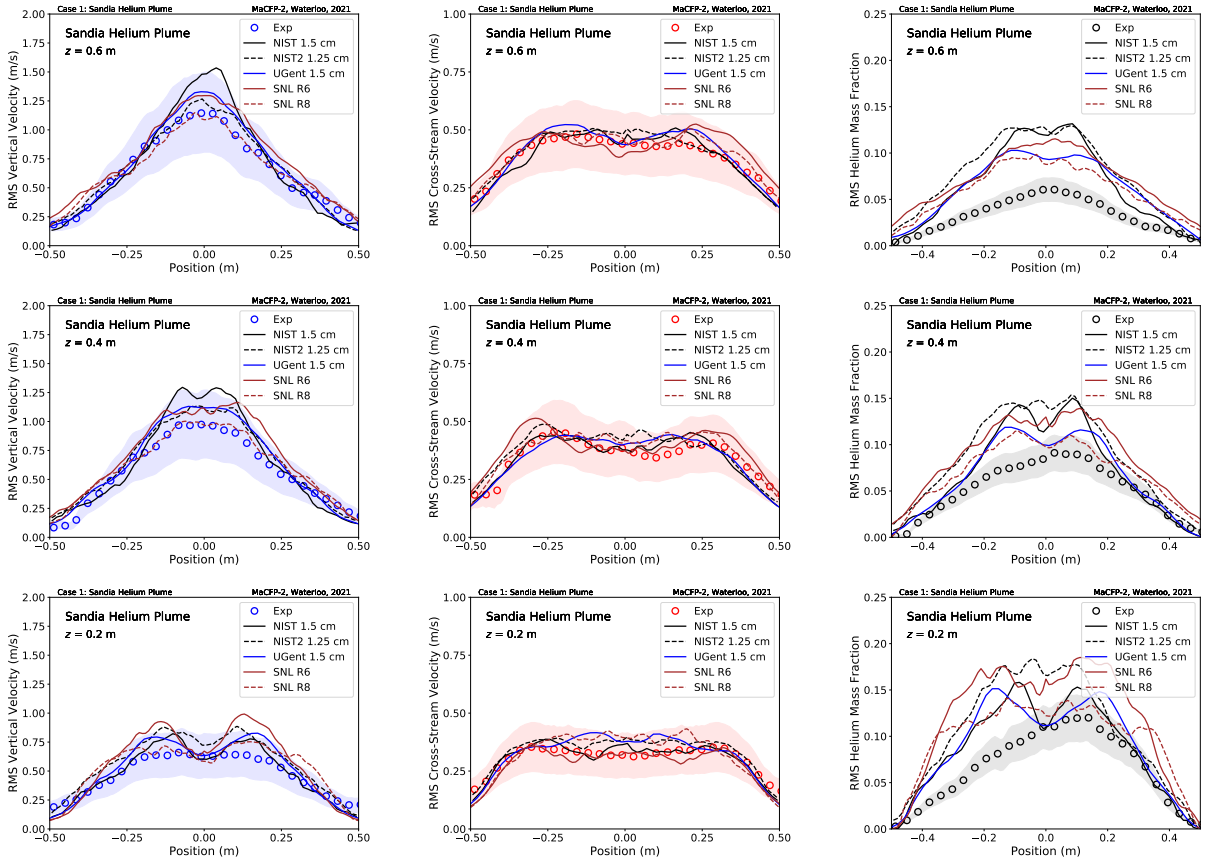

Figure 3: Sandia Helium Plume rms simulation results (nominally 1 cm - 1.5 cm resolution) at heights of 0.2, 0.4, and 0.6 m above the ground plane. Lightly colored region corresponds to experimental uncertainty obtained from [31].

rather than He/Acetone mass fraction (in contrast to the common belief at MaCFP 1). The third question motivated the submission of the "NIST2" simulation results.

The main findings at MaCFP-2 are as follows:

- Not focusing on the puffing frequency, general improvement in modeling results has been noted when comparing MaCFP-1 and MaCFP-2 results. In part, this may be attributable to improved turbulence models for certain codes (e.g., UGent introduced dynamic closures for momentum and scalars). In particular, the mean values (vertical and cross stream velocity; helium mass fraction) are well-captured on a mesh with resolution $D^*/\Delta x$ on the order of 10 (i.e., in line with engineering practice). Hence, if these mean values are the target of the simulations, current engineering practice with respect to mesh resolution is considered fine for this test case.

- The grid resolution requirement to accurately capture the plume dynamics, including the puffing frequency, was essentially confirmed, albeit that a 3 cm resolution seems sufficient ($D^*/\Delta x$ in the order of 35). This is significantly finer than engineering practice. It is noted that the UGent simulations do reveal a puffing phenomenon, but the amplitude at the dominant frequency is very low. It is also noted that, with the exception of NIST2, all simulation sets capture the puffing frequency accurately on a sufficiently fine mesh. The relatively strong deviation with the NIST2 settings suggests there is no advantage in modelling the entire set-up.

Table 4: Configuration and Global Burning Parameters for 30 cm Methanol Pool Fires

	UW [7]	NIST	Compilation
Burner ID (cm)	30.2	30.1	30
Burner Wall Thickness (mm)	1.3	1.5	various
Lip Height (mm)	10	10	5 to 10
Mass Flux (g/(m^2 s))	14.9	13.5 [32]	13.1 ± 0.9 [7, 32–42]
HRR (kW)	21.3	19.1 [32]	18.4 ± 1.3 [7, 32–42]
Puffing Freq (Hz)	2.8	2.64 [35]	2.8 ± 0.1 [7, 33, 35]

- With respect to the plume source, the dynamic approach (UGent results) seems to overcome the need for accurate inlet turbulence characteristics, whereas subgrid closure models that do not inherently promote hydrodyamic destabilization seem to require better inlet turbulence characterization. This said, at high grid resolution none of the simulation results are in good agreement with the rms value of the scalar concentration fluctuations, suggesting that plume source details might further improve the dynamic model results as well.

- It could not be concluded from the results whether a variable turbulent Schmidt number would have an important impact on the simulation results. A parameter study with constant Sc_t numbers could shed light on this.

- With increased grid resolution, the agreement for the velocity fields improves for all simulations, both in terms of mean and rms values. In contrast, and not yet fully understood, this is not the case for the rms of the scalar concentration fluctuations.

1.2. Case 3: Methanol Pool Fires

1.2.1. Experiments

The liquid pool fire experiment selected for the second MaCFP workshop is the same as the first MaCFP workshop: steadily-burning 0.30 m diameter methanol pool fires studied at the University of Waterloo (UW) [6, 7] and by staff and associates of the National Institute of Standards and Technology (NIST) [32–40]. The fires were established over liquid pan burners in a quiescent environment. The burners were operated at steady state conditions using gravity fuel feeds. The table below highlights the similarities and differences in the UW and NIST burner configurations and also lists a number of global parameters characterizing the fires. The height of the burner lip above the liquid fuel surface was generally 10 mm, but some earlier studies used 5 mm. The mass evaporation rate, averaging the results from 12 independent experimental campaigns and dozens of experiments was 13.1 g/(m^2 s), [7, 32–40] yielding a heat release rate of 18.4 kW and representing a fire Froude number[2], $\dot{Q}^*$, of about 0.33. The mean flame height was approximately 0.5 m [33]. The fire was characterized by a series of about 10 ribs and channels located near the base of the fire and anchored on the burner rim, growing and receding in tandem with the dynamic puffing instability of the fire. The dominant puffing frequency was about 2.8 Hz [7, 33, 35].

UW conducted time-resolved velocity (using two component, forward-scatter Laser Doppler Anemometry) and temperature (using 50 micron diameter, bare-wire Pt/Pt-10 % Rh thermocouples with 75-100 micron bead diameters) measurements in the highly-fluctuating region of the flame, i.e., up to radial positions located 16 cm from the pool fire centerline and up to 30 cm vertical elevation. Direct and Schlieren photography of the luminous flame were used to characterize the macroscopic and oscillatory behavior of the flame.

[2]The fire's Froude number is $\dot{Q}^* = \dot{Q}/(\rho_\infty c_p T_\infty \sqrt{g} D^{5/2})$.

Time series of data were ensemble-averaged to provide mean and rms values as well as correlation coefficients [7]. Errors in mean and rms velocities and mean temperatures were estimated as ± 5 % at 95 % confidence; errors in Reynolds stresses were estimated as ± 15 % at 95 % confidence [6]. Errors in rms temperatures and velocity-temperature correlations were difficult to estimate and were not quantified. No correction was made to temperature measurements for radiation or catalytic effects (estimated to be less than 5 %).

NIST measurements were complementary to those of UW. Several types of measurements were made including profiles of the total and radiative heat flux as a function of location just above the fuel surface. Measurements of radiative flux were made along a cylindrical control surface external to the fire, allowing estimation of the radiative fraction of the fire. This type of multi-location heat flux measurement, along with far-field single-location heat flux measurements, yielded a radiative fraction equal to 0.22 ± 0.02 [32–34, 36, 37]. Fine wire thermocouple and bidirectional probe measurements were made along the central axis of the fire to determine the temperature and gas velocity in the upward direction for distances as large as three diameters above the fire [43]. Thermocouple measurements were corrected for radiative loss. Based on thermocouple measurements in the burning fuel, the fuel surface temperature can be taken as close to the liquid boiling point. [43].

Additional measurements on the global and local structure of 30 cm diameter methanol, acetone, ethanol liquid pool fires and 37 cm diameter methane and propane pool fires are available and could be considered for future MaCFP validation exercises [39]. Measurements in all of these pool fires include profiles of chemical species above the fire centerline using extractive sampling and GC/MS analysis, centerline temperature and velocity profiles, and the distribution of heat fluxes emitted from the fires. The time dependent fuel temperatures at various locations within the liquid pools were also measured [39]. Analogous measurements in a 100 cm methanol pool fire provide insight on the impact of scale on these fires [43, 44]. In addition, the phase-dependent averaged temperature field in the 100 cm methanol pool fire was measured using thin filament pyrometry, which provides information on the complex dynamics associated with the puffing oscillations.

1.2.2. Simulations

The following groups submitted computational results:

- Electricité de France and Aix-Marseille University (EDFAMU)
- FM Global (FMGlobal)
- Ghent University (UGent)
- The National Institute of Standards and Technology (NIST)
- Sandia National Laboratories (Sandia)
- University of Maryland (UMD)
- University of New South Wales (UNSW)
- University of Warwick (UoW)

These groups used one of the following CFD solvers:

- Code_Saturne, version 5.0.9;
- FDS, version v6.7.5;

- FireFOAM, version v2012, v1912, 2.2.x, dev, or UoW;
- fireFPVFoam;
- SIERRA/Fuego, version 4.58.3.

Table 5 presents the main features of the numerical simulations performed by the different groups that submitted computational results. In Table 5, spatial resolution refers to the size of grid cells inside the flame region; and angular resolution refers to the number of solid angles used in the discretization of angular space in the radiation solver. RCFSK stands for the Rank Correlated Full Spectrum k-distribution model; PGRF stands for a prescribed global radiant fraction model; WSGG stands for a Weighted-Sum-of-Grey-Gases model. Pool BCs designate the different options for pool surface boundary conditions (BCs): prescribed or predicted mass loss rate (MLR); wall-resolved or wall-modeled Large Eddy Simulation (LES). In that terminology, wall-resolved LES are simulations in which the sharp gradients of radial velocity and temperature near the pool surface are captured by a sufficiently fine computational grid and no additional model is required to calculate the surface shear stress and convective heat flux. In contrast, wall-modeled LES are simulations in which the sharp gradients of radial velocity and temperature near the pool surface are unresolved by the computational grid and subgrid-scale models (often called wall functions) are required to reconstruct the surface shear stress and convective heat flux.

Overall, simulations provide a relatively accurate description of the large-scale puffing instability that is observed to dominate the unsteady behavior of the Case-3 pool flame. The simulated value of the instability frequency ranges between 2.4 Hz to 4 Hz whereas experimental measurements suggest a value between 2.6 Hz and 2.8 Hz.

Similarly, simulations that predict rather than prescribe the global radiant fraction, χ_{rad}, provide a relatively accurate (*i.e.* within 20%) description of global radiant emissions. The simulated value of χ_{rad} ranges between 0.18 to 0.26 whereas experimental measurements suggest a value of 0.22.

Simulations that predict rather than prescribe the fuel evaporation rate provide a relatively accurate (*i.e.,* within 20-25%) description of MLR. The simulated value of MLR ranges between 0.81 kg/s to 1.17 kg/s whereas experimental measurements suggest a value of 1.07 kg/s. A single recommendation (i.e., modeling decision) cannot be made to address this variability; instead, model sensitivity analysis is planned for the MaCFP-3 Workshop to assess its primary causes, including contributions from condensed phase (e.g., in-depth radiation absorption) and gas phase behaviors (e.g., soot formation and radiation emissions).

In general, it is found that models successfully simulate the main features of spatial variations of temperature, radial and vertical velocity, both for mean quantities and fluctuation intensities (*i.e.* root-mean-square values). An important question (perhaps the most important question in studies of Case 3) is whether the simulations are capable of accurately simulating the gas-to-liquid thermal feedback. Figure 4 presents detailed results for the mean total and radiative heat fluxes near the pool surface and shows that simulations reproduce the experimental variations with a 25-30% accuracy. In Case 3, the relative contributions of radiation/convection to the integrated rate of heat transfer to the pool surface are approximately 75%/25%.

In terms of radiation modeling, it is found that advanced gas radiation models (i.e. RCFSK, WSGG, and the box model) are competitive with the traditional approach based on a prescribed global radiant fraction, and that these models are more accurate than gray models.

Furthermore, it was found that these encouraging results were obtained provided that the simulations used sufficient spatial resolution. In the wall-resolved LES approach, grid convergence was obtained for 5-mm grid resolution, which was explained by the need to capture the gradients associated both with the small buoyancy-driven structures observed at the base of the pool flame and with the thin boundary layer observed at the surface of the liquid pool (these characteristic features have a size on the order of 1-2 cm). In the wall-modeled LES approach, grid convergence was obtained at 10-mm grid resolution (i.e., $D/30$), but not at 20-mm grid resolution (i.e., $D/15$), which suggests that in the current state of the art, wall models

Table 5: Main features of simulation database for Case 3

Name	Code	Spatial & angular resolution	Subgrid-scale models
EDFAMU	Code_Saturne	5-mm; 4608 angles	Turbulence: dynamic Smagorinsky, Pr_t, Sc_t Combustion: steady laminar flamelet model Radiation: RCFSK Pool BCs: prescribed MLR, wall-resolved LES
FMGlobal-1	FireFOAM	5-mm; 128 angles	Turbulence: dynamic k-eqn; $Pr_t = Sc_t = 1$ Combustion: Eddy Dissipation Model Radiation: PGRF or box model Pool BCs: prescribed MLR, wall-resolved LES
FMGlobal-2	FireFOAM	2.5, 5, 10-mm; 16 angles	Turbulence: dynamic k-eqn; $Pr_t = Sc_t = 1$ Combustion: Eddy Dissipation Model Radiation: PGRF Pool BCs: predicted MLR, wall-modeled LES
NIST	FDS	5, 10, 20-mm; 104 angles	Turbulence: Deardorff/WALE; $Pr_t = Sc_t = 0.5$ Combustion: two-step Eddy Dissipation Model Radiation: PGRF or gray model Pool BCs: prescribed or predicted MLR, wall-modeled LES
Sandia	SIERRA/Fuego	5 or 10-mm; 128 angles	Turbulence: k-equation model; $Pr_t = Sc_t = 0.9$ Combustion: laminar flamelet model Radiation: gray model Pool BCs: prescribed or predicted MLR, wall-resolved LES
UGent	FireFOAM	5, 10, 20, 30, 60-mm; 48 angles	Turbulence: dynamic Smagorinsky, Pr_t, Sc_t Combustion: Eddy Dissipation Model Radiation: PGRF or WSGG model Pool BCs: prescribed MLR, wall-modeled LES
UMD	FireFOAM	2.5, 5, 10-mm; 64 angles	Turbulence: dynamic k-eqn; $Pr_t = Sc_t = 0.5$ Combustion: Eddy Dissipation Model Radiation: PGRF or WSGG model Pool BCs: prescribed MLR, wall-resolved LES
UNSW	fireFPVFoam	10, 13.3, 20-mm; 64 angles	Turbulence: dynamic k-eqn; $Pr_t = Sc_t = 0.7$ Combustion: unsteady laminar flamelet model Radiation: PGRF model Pool BCs: prescribed MLR, wall-resolved LES
UoW	FireFOAM	5, 10, 20-mm; 80 angles	Turbulence: dynamic k-eqn; $Pr_t = Sc_t = 0.7$ Combustion: extended EDC model Radiation: gray model Pool BCs: predicted MLR, wall-modeled LES

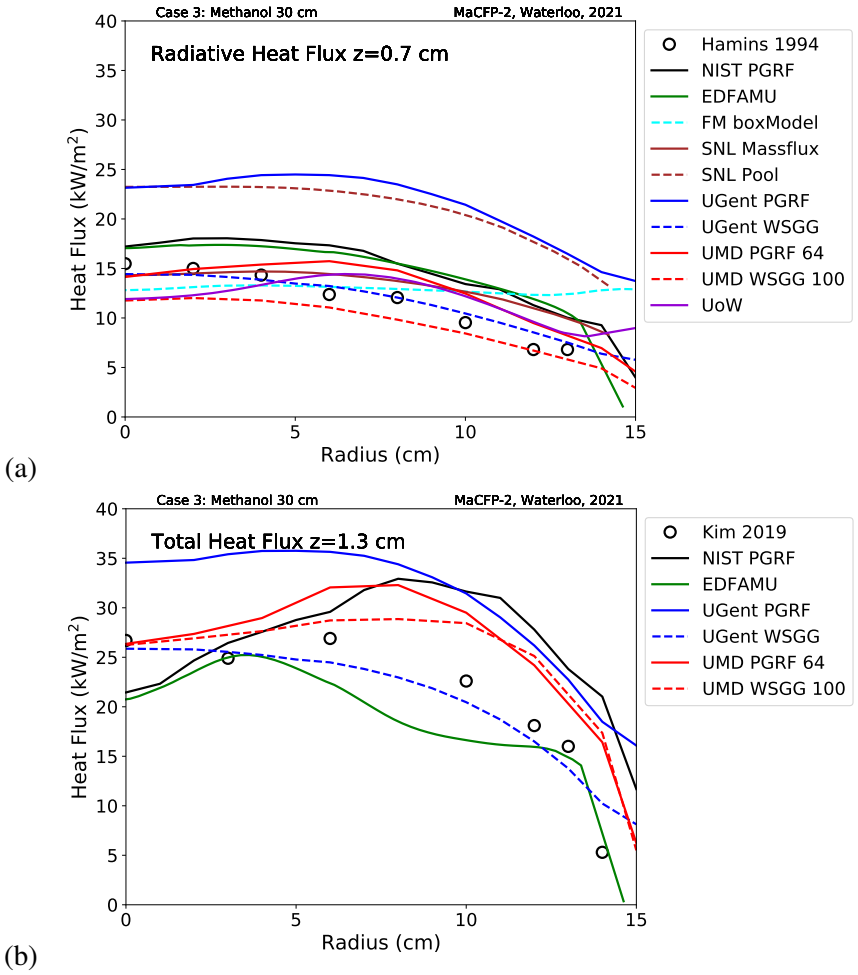

Figure 4: Radial variations of the intensity of the thermal feedback near the pool surface: (a) Radiative heat flux measured at 0.7 cm elevation above the pool; (b) Total heat flux measured at 1.3 cm elevation above the pool. Comparisons are between experimental data (symbols) and numerical simulations (lines) at the finest resolution submitted by the participant (see Table 5).

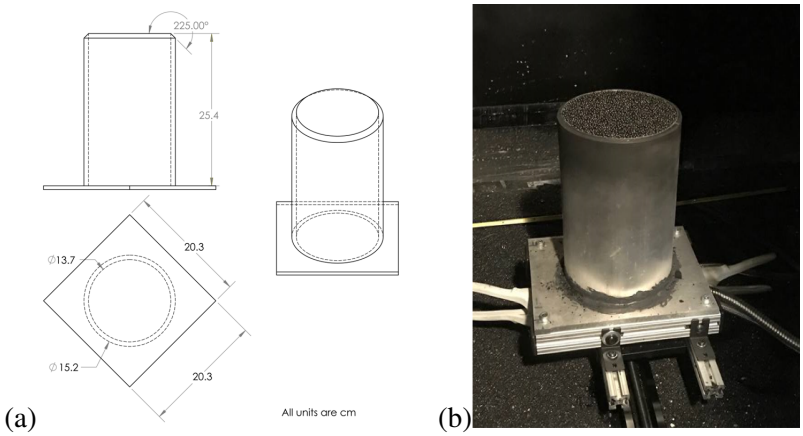

(a) (b)

Figure 5: FM Burner design.

allow a gain in computational time by a factor of approximately 10, but fail to provide accurate results for the type of computational grids that would be typically used by CFD practitioners (i.e., $D/10$).

1.2.3. Summary

Studies of Case 3 reveal that pool fires feature large length scales dynamics with flow/flame structures that have a size comparable to the diameter of the pool as well as small length scales dynamics with flow/flame structures associated with buoyancy-driven Rayleigh-Taylor instabilities or the thin pool-surface boundary layer, and that have a size of order 1 cm. The ability to correctly represent the small length scales dynamics is a key factor in accurate simulations of the gas-to-liquid thermal feedback. Results presented in MaCFP-2 suggest that it is important to differentiate between wall-resolved and wall-modeled LES. In wall-resolved LES simulations, accurate grid-converged solutions were obtained at 5-mm grid resolution; the thermal feedback is then predicted with approximately 25-30% accuracy. In wall-modeled LES simulations, accurate grid-converged solutions were obtained at 10-mm grid resolution; the thermal feedback is then predicted with approximately 25-30% accuracy. Results obtained at 20-mm (or coarser) resolution were mixed and were typically not accurate and/or not converged.

1.3. Case 5: FM Burner

1.3.1. Experiment

Flame temperature, soot volume fraction, soot radiation, and extinction of ethylene diffusion flames (co-flow) burning in air or reduced oxygen environments were measured using the burner design and boundary conditions described below. Figure 5 shows the burner geometry. The burner has an inner diameter of 13.7 cm and an outer diameter of 15.2 cm. The burner wall has a thickness of 1.5 cm and is water cooled to be approximately 25 °C. The upper outer edge is chamfered 45°. The burner surface is filled with steel beads, see Fig. 5, that are cooled by a cooling water coils placed inside steel beads.

Figure 6 shows the enclosure drawing. The enclosure has a cross section of 122 cm by 122 cm. The lower section is a plenum space and a sand bed for distributing the oxidizer. The burner placed on a translation stage sits above the sand bed, with the bottom surface of burner approximately 11.4 cm above the bed surface. The burner centerline is aligned with the exhaust hood at the start of a test, and could traverse laterally in an optical based experiment, e.g., laser induced incandescence measurements. The distance between the burner surface and hood lower edge is approximately 81 cm. The hood has an outer diameter of 61 cm. The exhaust flow rate is maintained at approximately 0.11 m^3/s. At this condition, the oxygen concentrations around the flame at various heights was verified to be the same as prescribed.

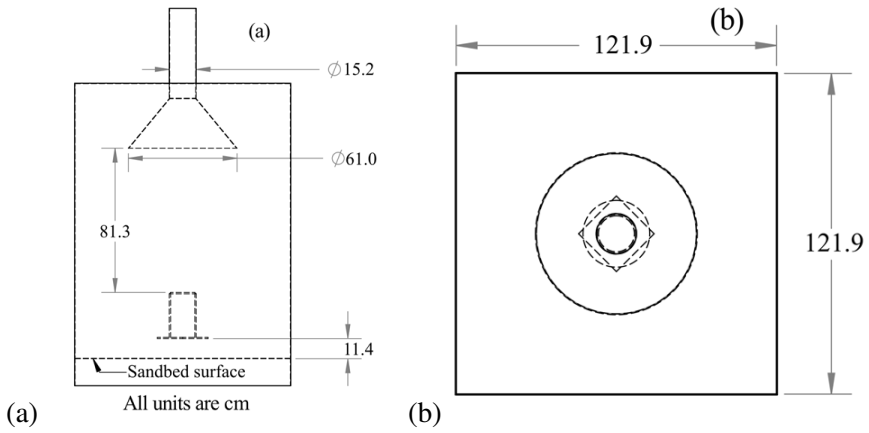

Figure 6: FM Burner compartment dimensions.

Table 6: Fuel and Oxidizer Flow Rate

Oxygen Concentration (Vol %)	Y_{O_2} Oxidizer (Mass fraction)	Ethylene Flow Rate (g/s)	Radiant Fraction
20.9	0.231	0.318	0.34
16.8	0.187	0.318	0.30
15.2	0.170	0.318	0.22

The flame examined in this study has a theoretical heat release rate of 15 kW. Three ambient (i.e., enclosure) oxygen concentrations (OC) are investigated, including normal air (20.9 % oxygen by volume), 16.8 % and 15.2 % oxygen in nitrogen. The fuel flow rates and corresponding oxygen concentrations are listed in Table 6. The total flow rate of oxidizer (i.e., air and nitrogen) under each OC condition is 3650 ± 250 L/min. The corresponding nominal velocity normal to the sand bed is 0.041 ± 0.003 m/s. The oxygen concentration in the co-flow is monitored using a gas analyzer, and verified at different locations around the flame (i.e., 30 cm radial distance from the burner centerline, and -5 cm, 20 cm, 46 cm, and 71 cm height from the burner surface, respectively). The change of oxygen concentration does not exceed 0.1 vol %.

Flame temperature measurements were recorded at 11 radial locations (r = 0 to r = 11 cm) across the width of the flame, at 6 heights above the top of the burner (66 total measurement locations). Temperature was measured using a two-thermocouple probe, and the reported data is corrected for radiation. This technique is mainly applied to correct the thermal inertia as the radiation correction for a small thermocouple junction is relatively small. The two thermocouples have nominal wire sizes of 25 and 50 microns.

Soot volume fraction was derived by two techniques — either radiation probe data or Laser Induced Incandescence (LII) data — assuming 9.5 as a dimensionless extinction coefficient based on Williams' study [45, 46] and 7.6 as the dimensionless absorption coefficient assuming 20 % scattering. In Williams' study [45, 46], a soot density value of 1.74 g/cm^3 is used to derive the 9.5 value for dimensionless extinction coefficient. Therefore, a soot density of 1.74 g/cm^3 should be used when converting soot mass fraction to volume fraction. Global radiant fraction was obtained by integration of mean vertical profiles of radiative heat flux.

1.3.2. Simulations

The following groups submitted simulation results:

- National Institute of Standards and Technology (NIST);
- University of Maryland (UMD);

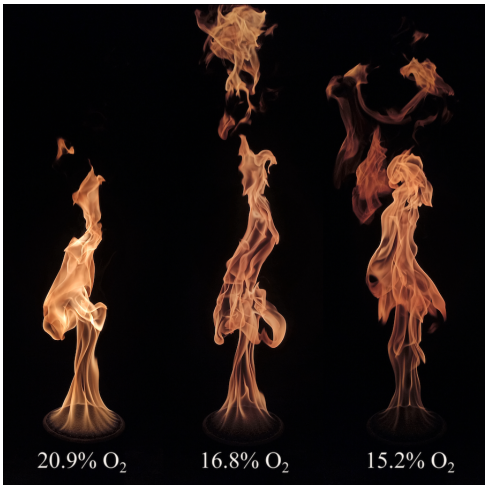

Figure 7: FM Burner flame images.

- Ghent University (UGent);
- University of Connecticut (UConn).

Key model setup parameters are provided in Table 7; detailed model descriptions (i.e., boundary & initial conditions, submodels, discretization, resolution and computational cost) are available on the MaCFP repository [23]. It is worth mentioning that the UGent simulations did not include any soot model and the UConn results were not fully converged due to too short calculation times. The UConn results were only first order accurate. No mesh sensitivity analysis was performed for the UMD or the UConn simulations, but the mesh cell size (0.5 cm for UMD and 0.35 cm for UConn) was similar to the finest meshes of the NIST and UGent results. The latter compared results on 3 meshes (2 cm, 1 cm and 0.5 cm), with local refinement in the UGent results and uniform mesh for the NIST results. UConn and UGent did not submit any results for cases with extinction (i.e., only the case with air as co-flow was considered by those groups).

A subset of computational results is shown below. Mean vertical profiles of radiant emission for two oxygen concentrations are shown in Fig. 8. Comparison of global radiant fraction with the integrated radiation profiles is shown in Table 8. Mean and rms temperature and soot volume fraction are provided below in Figs. 9 and 10. Note that data and results are also available for other axial distances from the burner and for additional coflow oxygen concentrations. The interested reader may find these results on the MaCFP GitHub repository [23].

1.3.3. Summary

A brief overview of the major observations is presented. With respect to the mean radiation emission as a function of height:

- There is a very strong mesh sensitivity of the results and no mesh convergence could be demonstrated.
- There is a significant impact of the radiation model.
- Only the NIST results reproduced the profiles qualitatively, on the finest mesh only.
- The overall reduction in radiation emission for reduced oxygen concentration is captured qualitatively.

The NIST predictions of the radiative fraction are in reasonable agreement with the experimental data. Only 2 oxygen concentrations were considered by UMD, and also in those results the reduction in radiative fraction for reduced oxygen concentration was well-captured.

Table 7: Model Parameters for FM Burner Simulations

Name	Code	Spatial & angular resolution	Subgrid-scale models
NIST	FDS v6.7.5	0.5, 1.0, and 2.0 cm 104 solid angles	Turbulence: modified Deardorff (algebraic model for k_{sgs}; $Pr_t = Sc_t = 0.5$) Combustion: 2-step serial model (60% CO and 40 % soot yield in the first reaction), combined with a critical temperature for flame extinction Radiation: predicted radiative fraction (using RADCAL) Soot: included in the combustion model
UConn	OpenFoam-5.x In house solver based on fireFOAM and reactingFOAM	0.35 cm	Turbulence: 1-eqn. model ($C_k = 0.03$, $Pr_t = Sc_t = 1.0$) Combustion: finite-rate chemistry with 32 species Radiation: optically thin with LBL (line-by-line) database Soot: empirical 2-equation model by Leung [47] with modified oxidation (including O and OH radicals) and tuned reaction rates
UGent	FireFOAM v2.2.x	0.5, 1.0, and 2.0 cm 48 solid angles	Turbulence: dynamic Smagorinsky (variable Pr_t, Sc_t) Combustion: Eddy-Dissipation Model, EDM ($C_{EDM} = 2$) Radiation: prescribed radiative fraction ($\chi_r = 0.34$) Soot: no soot model
UMD	FireFOAM v16.12.08	0.5 cm 72 solid angles (with fvDOM)	Turbulence: dynamic 1-eqn. model ($Pr_t = Sc_t = 0.5$) Combustion: Eddy-Dissipation Model, EDM ($C_{EDM} = 4$) Radiation: WSGGM (4 gray gases plus 1 transparent (with H_2O and CO_2 for gas) plus 2 gray gases for soot; results also submitted with predicted global radiative fraction ('PGRF') Soot: Laminar Smoke Point (LSP) based model

Table 8: Comparison of predicted and measured radiative fraction for FM Burner.

Oxygen [vol. %]	Measured Value	NIST	UMD
20.9	0.34	0.31	0.41
19.0	0.32	0.28	
16.8	0.30	0.26	
15.0	0.22	0.21	0.26

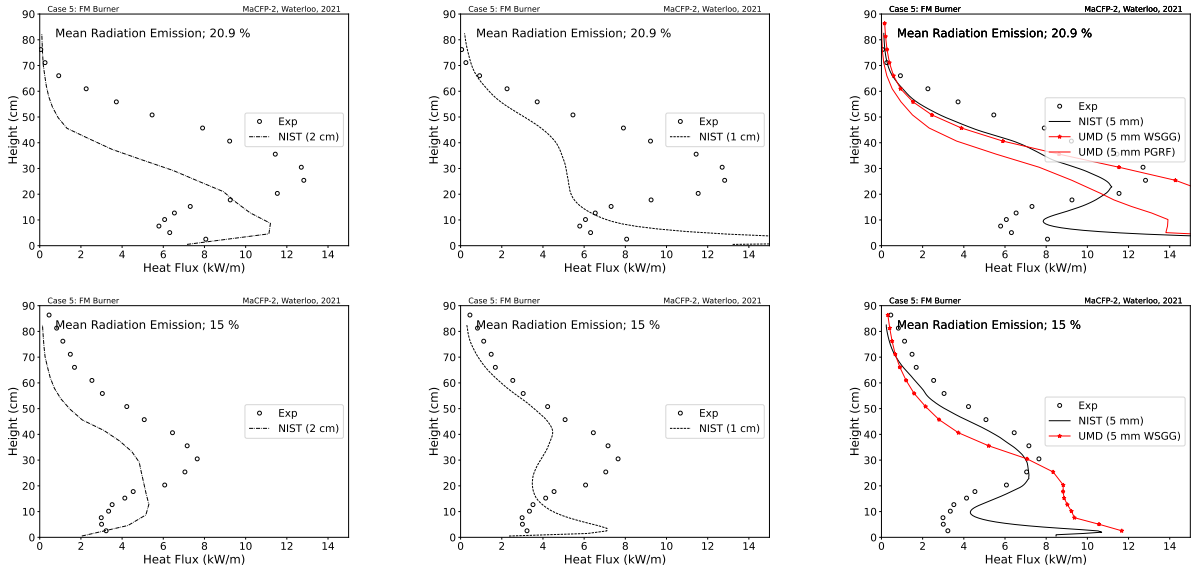

Figure 8: FM Burner, mean vertical radiant emission. Top row in air, bottom row at 15.2 vol. % O_2; from left to right, grid resolution increases from 2.0 cm to 0.5 cm.

With respect to radial profiles of mean and rms temperature at different heights, the NIST and UGent results show strong mesh sensitivity, even for mean temperature. The UGent results are somewhat less mesh sensitive, which might relate to the fully dynamic approach, but this remains to be confirmed in future simulations. In the UMD results the mean temperature drops too quickly as a function of height. The rise in mean temperature in the region between $1.0D$ and $1.5D$ height is captured qualitatively in the NIST and UGent results only. In general, the rms values for the temperature fluctuations are significantly higher in all simulation results than the experimental data (and the UGent profiles are too "flat").

Interestingly, for combustion with air, the results for the soot volume fraction (SVF) reveal less mesh sensitivity close to the burner, but the sensitivity increases further away. Only NIST results were available for the discussion of mesh sensitivity. Close to the burner all simulations over-predict the mean SVF significantly. Further away from the burner the agreement of the NIST results with experimental data improves, whereas the UMD results remain too high. The UMD results also reveal a very significant impact of the radiation model on the SVF results (mean and rms). The NIST results also provide rms values in good agreement with experimental data. With reduced oxygen concentration it is interesting to note that the NIST and UMD results are close to each other (and much higher than experimental data) for mean SVF close to the burner, but the rms values are much higher in the UMD results. Further away the differences between the NIST and UMD results become larger, the NIST profiles being better (and qualitatively in better agreement with the experiments). The overall reduction in mean SVF with reduced oxygen concentration is not well captured in the simulations. In general, the large deviations between the simulation results and experimental data for mean SVF remain to be explained, particularly because the agreement for the radiative fraction was so good.

Combustion efficiency was reported by NIST who used the critical flame temperature approach for extinction. The values NIST used for CFT of each fuel were taken from the SFPE handbook [48]: 1337 °C for ethylene, 1427 °C for propylene, 1447 °C for propane, and 1507 °C for methane. Results for these four fuels at three grid resolutions are shown in Fig. 11.

In the closing discussion for this case it was mentioned that:

- Strong intermittency effects were reported in the analysis of the experimental data, which might pose

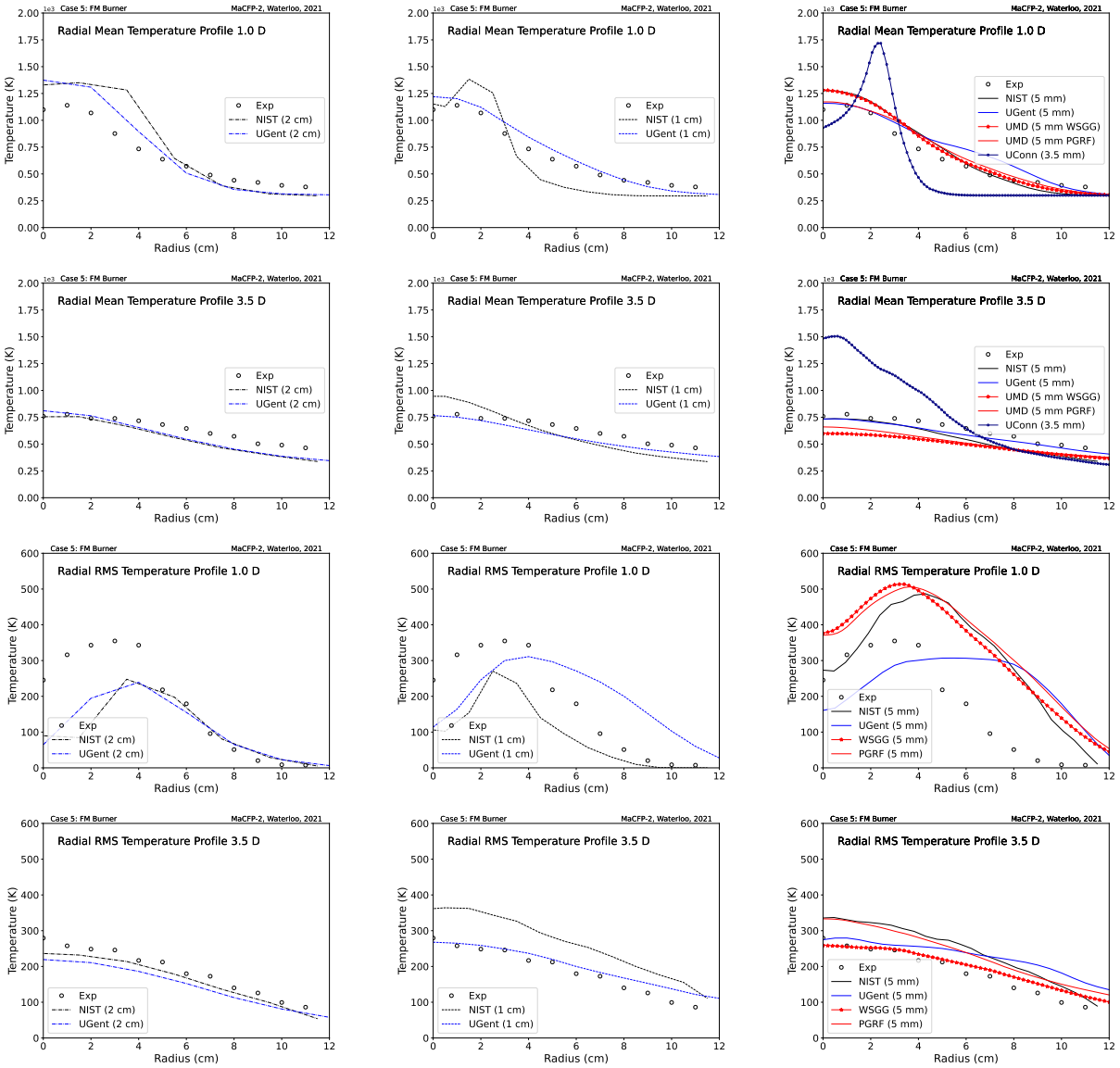

Figure 9: FM Burner, mean (top two rows) and rms (bottom two rows) temperature profiles for 1 D (burner diameter) and 3.5 D axial distance from the burner in air (20.9 vol. % O_2). Left column shows model results at 2 cm resolution; middle column shows 1 cm resolution; and right column is 5 mm resolution.

additional challenges on numerical simulations;

- PDFs of soot volume fraction and temperature and soot concentration correlations are available and it was suggested to expand the discussion of CFD results in that sense;
- The combustion efficiency was only explored by one group with one model at MaCFP-2; further analysis of this dataset is recommended for future work;
- Given the wide variety in choices made for all models (turbulence, combustion, radiation, soot) no decisions could be made yet in terms of recommendations.

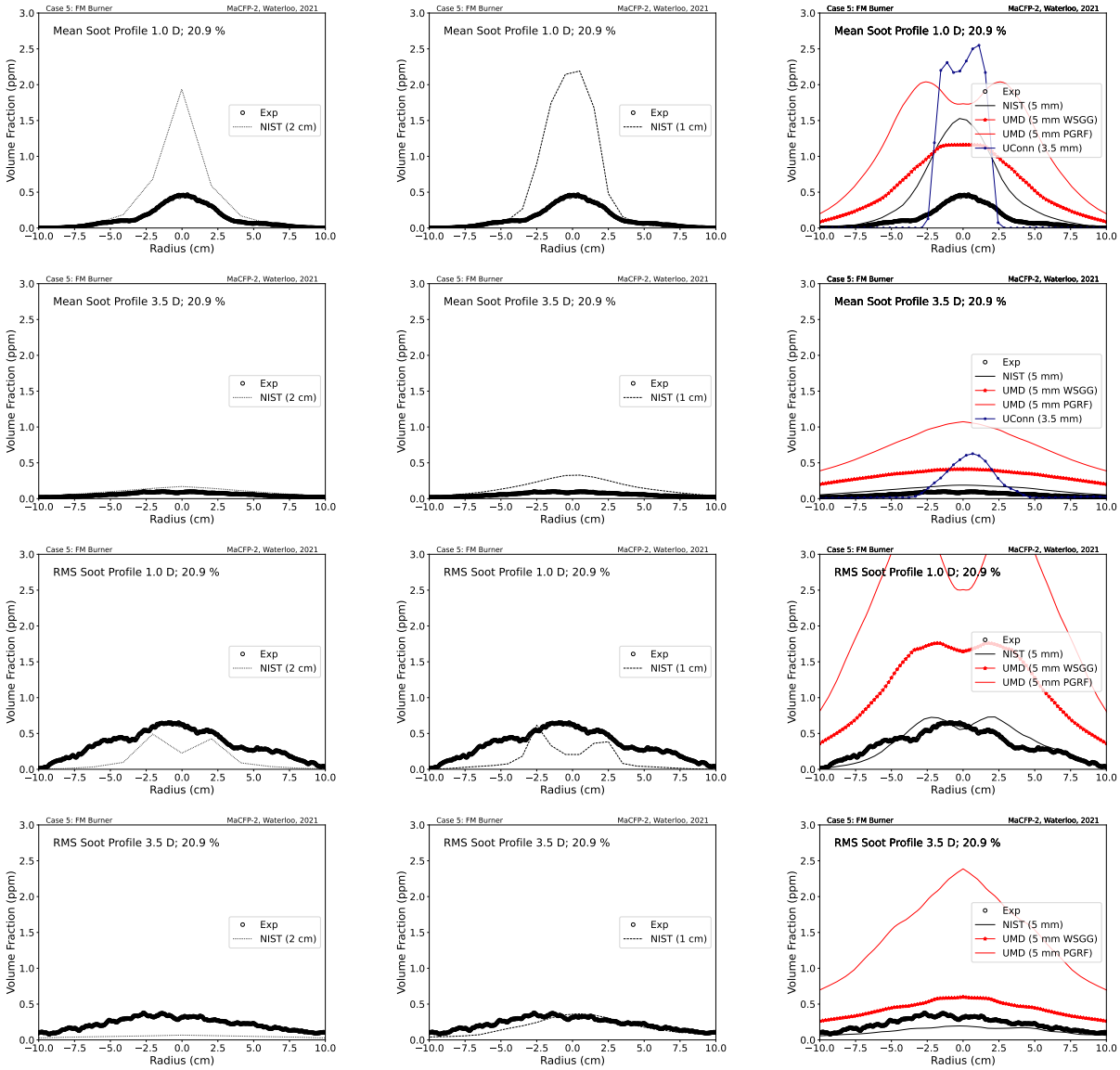

Figure 10: FM Burner, mean (top two rows) and rms (bottom two rows) profiles of soot volume fraction for 1 D (burner diameter) and 3.5 D axial distance from the burner in air (20.9 vol. % O_2). Left column shows models results at 2 cm resolution; middle column shows 1 cm resolution; and right column is 5 mm resolution.

1.4. Current and Future Plans

Compared to MaCFP-1, MaCFP-2 has seen significant progress made in simulations of radiant emissions showing some encouraging success in *predicting* rather than *prescribing* the global radiative loss fraction. In particular, significant progress has been made in simulations of gas radiation in non-sooting flames (Case 3), in particular in the representation of spectral effects by non-gray models. However, predicting soot volume fractions and soot radiation remains a challenge (Case 5).

Compared to MaCFP-1, MaCFP-2 has seen several attempts by computational modeling groups to consider both fine-grained simulations that are often used in research-level projects and coarse-grained simulations that are more typical of engineering-level projects (Case 3). Results are mixed, which suggests that the

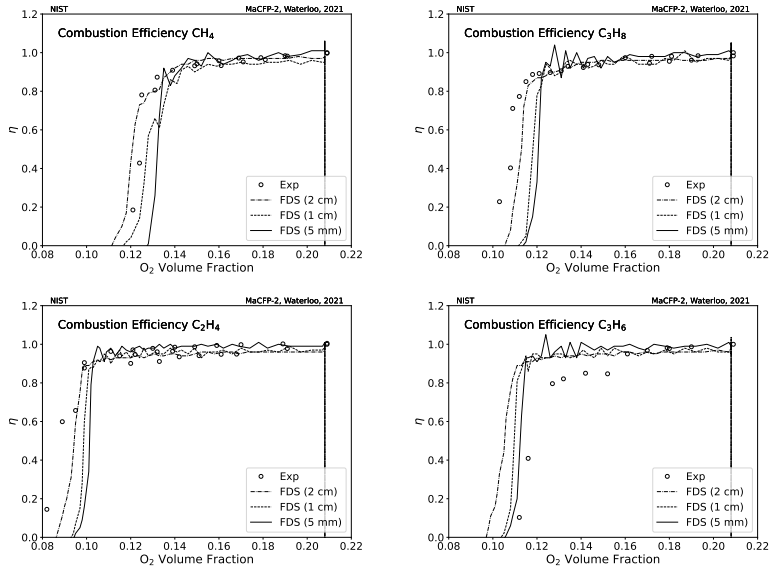

Figure 11: FM Burner combustion efficiency.

development of the wall functions that are required to describe heat and mass transfer along fuel surfaces in coarse-grained simulations remains a challenge. Different features of each target case were shown to require unique mesh resolutions for accurate results; hence, depending on the target value of interest for a given simulation, engineering guidelines for mesh resolution (i.e., $D^*/\Delta x$ on the order of 10) may or may not be sufficient.

- Specifically, for Case 1 (Helium plume), $D^*/\Delta x = 10$ is sufficient for mean vertical and cross stream velocity and mean helium mass fraction; however, $D^*/\Delta x = 35$ is needed to accurately capture puffing frequency. With increased mesh resolution, the agreement for the velocity fields improves for all simulations, both in terms of mean and rms values; in contrast, and not yet fully understood, agreement does not improve for the rms of the scalar concentration fluctuations.

- For Case 3 (methanol pool fire), simulation results suggest that it is important to differentiate between wall-resolved and wall-modeled LES. To predict flame-to-pool thermal feedback with approximately 25% to 30% accuracy, accurate grid-converged solutions were obtained (a) for wall-resolved LES simulations, at 5-mm mesh resolution and (b) for wall-modeled LES simulations at 10-mm mesh resolution.

- For Case 5 (FM Burner), with respect to mean radiant emissions, there is a very strong mesh sensitivity of the results and no grid-convergence could be demonstrated. With respect to radial profiles of mean and rms temperature at different heights, the NIST and UGent results show strong mesh sensitivity (though UGent results are somewhat less mesh sensitive, potentially related to the fully dynamic approach used). Notably, for combustion with air, predicted soot volume fraction (SVF) demonstrates less mesh sensitivity near the burner, but increased sensitivity farther away.

  Based on the results presented at MaCFP-2, further analysis of specific aspects of these datasets is recommended. In Case 5 (FM Burner), combustion efficiency was only explored by one group, with one model. More broadly, given the wide range of model choices (turbulence, combustion, radiation, soot) used in submitted results, no decisions could be made yet in terms of recommendations. This limitation is shared when considering predictions of thermal feedback and burning rate in the Case 3

(methanol pool fire). It is suggested that a constrained, systematic modeling analysis be conducted, whereby submodels (and/or related input coefficients) are systematically varied in order to assess their specific impact on global model predictions of interest. With regards to Case 3, a key extension of these results would be assessment of how these modeling decisions impact predictions of burning rate or fire growth: specifically, exploring the correlation between variability in model predictions of thermal feedback and burning rate.

The third MaCFP workshop (MaCFP-3) will feature comparisons of experimental data and computational results obtained in separate, decoupled, condensed-phase and gas-phase fire configurations, building upon the analysis and lessons learned of the MaCFP-2 Workshop. Additionally, MaCFP-3 will be the first MaCFP workshop to feature fully coupled cases corresponding to flame spread over a combustible solid. Current plans are to explore flame spread over the cast, black poly(methyl methacrylate), PMMA, characterized by the Condensed Phase Subgroup during MaCFP-2 [proceedings in preparation; preliminary summary of experimental measurements available online [49]]. Specifically, flame spread experiments of interest include (1) a 1.46 m corner wall configuration (based on the Single Burning Item (SBI) Test, EN13823 [50]) and (2) a 2.44 m parallel panel configuration studied (based on the FM4910 Parallel Panel Test [51]).

Acknowledgments

The authors would like to gratefully acknowledge the endorsement and support of MaCFP by IAFSS. The authors would also like to acknowledge all the researchers who contributed to the development of the experimental databases that were used in the present validation work, in particular the authors of Refs. [2–18, 21, 33–39, 43, 44]. Finally, the authors would like to gratefully acknowledge the contributions of all the researchers who contributed to the development of the numerical databases for the first MaCFP workshop, in particular the authors of Refs. [52–70].

References

[1] A. S. Brown, M. Bruns, M. Gollner, J. C. Hewson, G. A. Maragkos, A. Marshall, R. McDermott, B. Merci, T. Rogaume, S. I. Stoliarov, J. L. Torero, A. Trouvé, Y. Wang, E. J. Weckman, Proceedings of the First Workshop Organized by the IAFSS Working Group on Measurement and Computation of Fire Phenomena (MaCFP)., Fire safety journal 101 (2018).
URL https://doi.org/10.1016/j.firesaf.2018.08.009 2, 3, 6

[2] T. J. O'Hern, E. J. Weckman, A. L. Gerhart, S. R. Tieszen, R. W. Schefer, Experimental study of a turbulent buoyant helium plume, J. Fluid Mech. 544 (2005) 143–171. 2, 5, 6, 22

[3] B. J. McCaffrey, Purely buoyant diffusion flames: some experimental results, National Bureau of Standards, NBSIR 79-1910 (1979). 2

[4] S. R. Tieszen, T. J. O'Hern, R. W. Schefer, E. J. Weckman, T. K. Blanchat, Experimental study of the flow field in and around a one meter diameter methane fire, Combust. Flame 129 (2002) 378–391. 2

[5] S. R. Tieszen, T. J. O'Hern, E. J. Weckman, R. W. Schefer, Experimental study of the effect of fuel mass flux on a 1-m-diameter methane fire and comparison with a hydrogen fire, Combust. Flame 139 (2004) 126–141. 2

[6] E. J. Weckman, The structure of the flowfield near the base of a medium-scale pool fire, Ph.D. Thesis, University of Waterloo, ON, Canada (1987). 2, 3, 9, 10

[7] E. J. Weckman, A. B. Strong, Experimental investigation of the turbulence structure of medium-scale methanol pool fires, Combust. Flame 105 (1996) 245–266. 2, 3, 9, 10

[8] A. Hamins, S. J. Fischer, T. Kashiwagi, M. E. Klassen, J. P. Gore, Heat feedback to the fuel surface in pool fires, Combust. Sci and Tech. 97 (1994) 37–62. 2

[9] S. C. Kim, K. Y. Lee, A. Hamins, Energy balance in medium-scale methanol, ethanol, and acetone pool fires, Fire Safety J. 107 (2019) 44–53.

[10] A. Hamins, A. Lock, The structure of a moderate-scale methanol pool fire, NIST Technical Note 1928, National Institute of Standards and Technology, Gaithersburg (2016).

[11] R. Falkenstein-Smith, K. Sung, J. Chen, A. Hamins, Chemical structure of medium-scale liquid pool fires, Fire Safety J. 120 (2021) 103099. 2

[12] J. L. de Ris, G. H. Markstein, L. Orloff, P. A. Beaulieu, Flame heat transfer, part I: pyrolysis zone, Factory Mutual Research, Tech. Report J.I. 0D0J9.MT (1999). 2

[13] J. L. de Ris, G. H. Markstein, L. Orloff, P. A. Beaulieu, Similarity of turbulent wall fires, International Association for Fire Safety Science, Proc. Seventh Intl. Symposium (2003) 259-270. 2

[14] D. Zeng, P. Chatterjee, Y. Wang, The effect of oxygen depletion on soot and thermal radiation in buoyant turbulent diffusion flames, Proc. Combust. Inst. 37 (2019) 825–832. 2

[15] X. Ren, D. Zeng, Y. Wang, G. Xiong, G. Agarwal, M. Gollner, Temperature measurement of a turbulent buoyant ethylene diffusion flame using a dual-thermocouple technique, Fire Safety J. 120 (2021) 103061. 2

[16] J. P. White, Measurement and simulation of suppression effects in a buoyant turbulent line fire, Ph.D. thesis, University of Maryland, College Park, USA (2016). 2

[17] J. P. White, E. D. Link, A. C. Trouvé, P. B. Sunderland, A. W. Marshall, J. A. Sheffel, M. L. Corn, M. B. Colket, M. Chaos, H.-Z. Yu, Radiative emissions measurements from a buoyant, turbulent line flame under oxidizer-dilution quenching conditions, Fire Safety J. 76 (2015) 74–84.

[18] J. P. White, E. D. Link, A. C. Trouvé, P. B. Sunderland, A. W. Marshall, A general calorimetry framework for measurement of combustion efficiency in a suppressed turbulent line fire, Fire Safety J. 92 (2017) 164–176. 2, 3, 22

[19] I. Leventon, M. Heck, K. McGrattan, M. Bundy, R. Davis, The impact of material composition on ignitability and fire growth. volume 1: Full-scale burning behavior of combustible solids commonly found in nuclear power plants, Technical Note 2282, National Institute of Standards and Technology, Gaithersburg, Maryland (February 2024). 3

[20] I. Leventon, M. Heck, K. McGrattan, M. Bundy, R. Davis, Experimental measurements for fire model validation - parallel panel tests on pmma, National Institute of Standards and Technology MIDAS (2022).
URL https://data.nist.gov/od/id/mds2-2812 3

[21] D. M. Chaudhari, G. J. Fiola, S. I. Stoliarov, Experimental analysis and modeling of buoyancy-driven flame spread on cast poly(methyl methacrylate) in corner configuration, Polym. Degrad. Stab. 183 (2021) 109433. 3, 22

[22] I. Leventon, K. Lannoye, Experimental measurements for pyrolysis model validation - anaerobic gasification of pmma under external thermal radiation, National Institute of Standards and Technology MIDAS (2023).
URL https://data.nist.gov/od/id/mds2-2940 3

[23] https://github.com/MaCFP. 3, 6, 16

[24] Code_Saturne, developed by Electricité de France, see https://www.code-saturne.org. 4

[25] FDS, developed by the National Institute of Standards and Technology in collaboration with the VTT Technical Research Centre of Finland, available at: https://pages.nist.gov/fds-smv and https://github.com/firemodels/fds (accessed: 02-15-2018). 4

[26] OpenFOAM, developed by the OpenFOAM Foundation, available at: http://www.openfoam.org (accessed: 11-14-2017). 4

[27] FireFOAM, developed by FM Global, available at: https://github.com/fireFoam-dev (accessed: 02-15-2018). 4

[28] fireFPVFoam, developed by University of New South Wales. 4

[29] SIERRA/Fuego, developed by Sandia National Laboratories, see https://www.sandia.gov/vqsec/capabilities/companalysis/. 4

[30] T. Blanchat, Characterization of the air source and plume source at FLAME, Sandia National Laboratories, Report SAND01-2227 (2001). 5

[31] P. E. DesJardin, T. J. O'Hern, S. R. Tieszen, Large eddy simulation and experimental measurements of the near-field of a large turbulent helium plume, Physics of Fluids 16 (6) (2004) 1866–1883. 7, 8

[32] S. Kim, K. Lee, , A. Hamins, Energy balance in medium-scale methanol, ethanol, and acetone pool fires, Fire Safety Journal 107 (2019) 44–53. 9, 10

[33] A. Hamins, M. Klassen, J. Gore, S. Fischer, T. Kashiwagi, Heat feedback to the fuel surface in pool fires, Comb. Sci. Tech. 97 (1994) 37–62. 9, 22

[34] M. Klassen, J. Gore, Structure and radiation properties of pool fires, GCR 94-651, National Institute of Standards and Technology, Gaithersburg, Maryland (June 1994). 10

[35] Z. Wang, W. Tam, J. Chen, K. Lee, A. Hamins, Thin filament pyrometry field measurements in a medium-scale pool fire, Fire Technology 56 (2020) 837–861. 9

[36] A. Hamins, M. Klassen, J. Gore, T. Kashiwagi, Estimate of flame radiance via a single point location measurement in liquid pool fires, Combustion and Flame 86 (1991) 223–228. 10

[37] R. Buch, A. Hamins, K. Konishi, D. Mattingly, T. Kashiwagi, Radiative emission fraction of pool fires burning silicone fluids, Combust. Flame 108 (1997) 118–126. 10

[38] R. Falkenstein-Smith, K. Sung, J. Chen, A. Hamins, Chemical structure of medium-scale liquid pool fires, Fire Safety Journal 120 (2021) 103099.

[39] R. Falkesntein-Smith, K. Sung, J. Chen, K. Harris, A. Hamins, The structure of medium-scale pool fires, Technical Note 2082-rev2, National Institute of Standards and Technology, Gaithersburg, Maryland (January 2022; NIST TN 2082-rev3, in preparation, 2023). 10, 22

[40] A. Yilmaz, Radiation transport measurements in methanol pool fires with fourier transform infrared spectroscopy, GCR 09-922, National Institute of Standards and Technology, Gaithersburg, Maryland (August 2009). 9

[41] R. Corlett, T. Fu, Some recent experiments with pool fires, Pyrodynamics 1 (1966) 253–269.

[42] K. Akita, T. Yumoto, Heat transfer in small pools and rates of burning of liquid methanol, in: Proceedings of the Combustion Institute, Vol. 10, The Combustion Institute, 1965, pp. 943–948. 9

[43] K. Sung, J. Chen, M. Bundy, M. Fernandez, A. Hamins, The thermal character of a 1 m methanol pool fire, Technical Note 2083r1, National Institute of Standards and Technology, Gaithersburg, Maryland (June 2021). 10, 22

[44] J. Chen, K. Sung, Z. Wang, W. Tam, K. Lee, , A. Hamins, The evolving temperature field in a 1 m methanol pool fire, J Fire Sciences 39 (2021) 309–323. 10, 22

[45] T. Williams, C. Shaddix, K. Jensen, J. Suo-Anttil, Measurement of the dimensionless extinction coefficient of soot within laminar diffusion flames, Int. J. Heat and Mass Transfer 50 (2007) 1616–1630. 15

[46] M. Choi, G. Mulholland, A. Hamins, T. Kashiwagi, Comparisons of the soot volume fraction using gravimetric and light extinction techniques, Combust. Flame 102 (1995) 161–169. 15

[47] K. M. Leung, R. P. Lindstedt, W. P. Jones, A simplified reaction mechanism for soot formation in nonpremixed flames, Combustion and flame 87 (3-4) (1991) 289–305. 17

[48] C. L. Beyler, SFPE Handbook of Fire Protection Engineering, 4th Edition, National Fire Protection Association, Quincy, Massachusetts, 2008, Ch. Flammability Limits of Premixed and Diffusion Flames. 18

[49] B. Batiot, M. Bruns, S. Hostikka, I. Leventon, Y. Nakamura, P. Reszka, T. Rogaume, S. Stoliarov, Preliminary summary of experimental measurements: Predecisional draft report submitted to the 2021 MaCFP condensed phase workshop, https://github.com/MaCFP/matl-db/releases/download/v1.0.0/MaCFP_2021_Report_Part_I_Experimental.pdf, archived: https://perma.cc/T6LR-95A2. 22

[50] EN 13823:2020, Reaction to fire tests for building products - Building products excluding floorings exposed to the thermal attack by a single burning item. 22

[51] ANSI/FM 4910-2013 (2021), American National Standard for Cleanroom Materials Flammability Test Protocol ANSI/FM Approvals 4910. 22

[52] G. Boyer, First MaCFP Workshop – Case 1, Lund University, Sweden (2017). 22

[53] R. McDermott, First MaCFP Workshop – Case 1, Lund University, Sweden (2017).

[54] G. Maragkos, First MaCFP Workshop – Case 1, Lund University, Sweden (2017).

[55] O. Oluwole, First MaCFP Workshop – Case 2a, Lund University, Sweden (2017).

[56] G. Maragkos, First MaCFP Workshop – Case 2a, Lund University, Sweden (2017).

[57] G. Boyer, First MaCFP Workshop – Case 2a, Lund University, Sweden (2017).

[58] R. McDermott, First MaCFP Workshop – Case 2a, Lund University, Sweden (2017).

[59] G. Maragkos, First MaCFP Workshop – Case 2b, Lund University, Sweden (2017).

[60] R. McDermott, First MaCFP Workshop – Case 2b, Lund University, Sweden (2017).

[61] J. Hewson, H. Koo, First MaCFP Workshop – Case 2b, Lund University, Sweden (2017).

[62] D. Alvear-Portilla, M. Lázaro-Urrutia, A. Alonso-Ipiña, First MaCFP Workshop – Case 2b, Lund University, Sweden (2017).

[63] G. Maragkos, T. Beji, B. Merci, First MaCFP Workshop – Case 3, Lund University, Sweden (2017).

[64] A. Marchand, S. Verma, A.Trouvé, First MaCFP Workshop – Case 3, Lund University, Sweden (2017).

[65] T. Sikanen, First MaCFP Workshop – Case 3, Lund University, Sweden (2017).

[66] K. McGrattan, First MaCFP Workshop – Case 4, Lund University, Sweden (2017).

[67] N. Ren, First MaCFP Workshop – Case 4, Lund University, Sweden (2017).

[68] N. Ren, First MaCFP Workshop – Case 5, Lund University, Sweden (2017).

[69] R. McDermott, First MaCFP Workshop – Case 5, Lund University, Sweden (2017).

[70] A. Marchand, S. Verma, A. Trouvé, First MaCFP Workshop – Case 5, Lund University, Sweden (2017). 22